Freeze gelated porous membranes for periodontal tissue regeneration

Saad B. Qasim [a], Robin M. Delaine-Smith [b], Tobias Fey [c], Andrew Rawlinson [d], Ihtesham Ur Rehman [a],*

[a] Materials Science and Engineering Department, Kroto Research Institute, University of Sheffield, Sheffield S3 7HQ, United Kingdom
[b] Institute of Bioengineering, School of Engineering and Materials Science, Queen Mary University of London, Mile End Road, E1 4NS London, United Kingdom
[c] Department of Materials Science (Glass and Ceramics), University of Erlangen-Nuernberg, Martensstr. 5, 91058 Erlangen, Germany
[d] Academic Unit of Restorative Dentistry, School of Clinical Dentistry, University of Sheffield, Sheffield S10 2SZ, United Kingdom

A R T I C L E   I N F O

A B S T R A C T

Guided tissue regeneration (GTR) membranes have been used for the management of destructive forms of periodontal disease as a means of aiding regeneration of lost supporting tissues, including the alveolar bone, cementum, gingiva and periodontal ligaments (PDL). Currently available GTR membranes are either non-biodegradable, requiring a second surgery for removal, or biodegradable. The mechanical and biofunctional limitations of currently available membranes result in a limited and unpredictable treatment outcome in terms of periodontal tissue regeneration. In this study, porous membranes of chitosan (CH) were fabricated with or without hydroxyapatite (HA) using the simple technique of freeze gelation (FG) via two different solvents systems, acetic acid (ACa) or ascorbic acid (ASa). The aim was to prepare porous membranes to be used for GTR to improve periodontal regeneration. FG membranes were characterized for ultra-structural morphology, physiochemical properties, water uptake, degradation, mechanical properties, and biocompatibility with mature and progenitor osteogenic cells. Fourier transform infrared (FTIR) spectroscopy confirmed the presence of hydroxyapatite and its interaction with chitosan. μCT analysis showed membranes had 85–77% porosity. Mechanical properties and degradation rate were affected by solvent type and the presence of hydroxyapatite. Culture of human osteosarcoma cells (MG63) and human embryonic stem cell-derived mesenchymal progenitors (hES-MPs) showed that all membranes supported cell proliferation and long term matrix deposition was supported by HA incorporated membranes. These CH and HA composite membranes show their potential use for GTR applications in periodontal lesions and in addition FG membranes could be further tuned to achieve characteristics desirable of a GTR membrane for periodontal regeneration.

1. Introduction

Destructive forms of periodontal disease such as chronic periodontitis affect the supporting tissues of teeth causing loss of gingival tissue, connective tissue, alveolar bone and periodontal ligaments. Initial treatment of these diseases includes the elimination of the primary causative factor (the dental plaque biofilm) by effective patient performed oral hygiene procedures and non-surgical treatment provided by a dentist or hygienist. While treatment usually halts disease progression, healing is characterized by repair of affected tissues with a long junctional epithelium, bone remodeling, and limited regeneration of the cementum and the lost periodontal ligaments that normally attach the tooth to the alveolar bone.

For these reasons, there has been much interest in developing methods for enhancing the regeneration of lost tissues in order to restore dental function and esthetics. This has been met with limited success using biologically active agents and guided tissue regenerative (GTR) or guided bone regeneration (GBR) membranes [1,2]. The ideal requirements for a GTR membrane include; a cell isolating occlusive biomaterial which meets minimum mechanical, physical, structural and biocompatibility requirements; ability to support organized and vascularized ingrowth and wound stabilization; protecting the underlying blood clot and thereby limiting the epithelial and unwanted connective tissue growth into the defect; promoting functional tissue regeneration from the relevant cells in the defect (avoiding healing by repair); and degrading in adequate time to provide space for newly formed periodontal tissue. The membrane surface facing the soft tissue should support cell attachment, growth and differentiation while the surface facing the defect acts as a biological seal [3].

A number of resorbable GTR/GBR membranes have now replaced the conventional non-resorbable membrane (expanded

* Corresponding author at: The Kroto Research Institute, North Campus, University of Sheffield, Broad Lane, Sheffield S3 7HQ, United Kingdom. Tel.: +44 (0) 114 222 5946; fax: +44 (0) 114 222 5943.

E-mail address: i.u.rehman@sheffield.ac.uk (I.U. Rehman).

polytetraflouroethylene), which required a second stage surgical intervention to remove, resulting in damage to the newly formed tissue [4]. Many of the current resorbable membranes are based on the use of synthetic polyesters, such as, poly (lactic and glycolic acid) or polycaprolactone. Although these membranes have adequate mechanical and degradation profiles, they lack bioactivity [5,6]. The use of naturally occurring biopolymers, such as, collagen and chitosan (CH) has also been explored. Collagen based materials have shown favorable results due to excellent biocompatibility, however, there is batch variability and lack of control over the resorption rate which is a concern for clinicians. Moreover, the use of membranes derived from animal tissues is associated with the risk of disease transmission and has also raised certain ethical and cultural issues [7–9]. Using a functionally graded approach to fabricate a biomimetic GTR membrane has been proposed by Bottino et al. [2], which has the potential to fulfill all ideal GTR membrane criteria.

The use of CH as a potential biomaterial for tissue engineering and regenerative medicine has been investigated during the past 20 years. CH is produced by deacetylation of chitin, which is the second most abundant naturally occurring polysaccharide in nature. CH is a linear polysaccharide copolymer of β-(1-4) linked D-glucosamine and N-acetylated-D-glucosamine making up deacetylated and acetylated regions respectively [8,10–12]. The amide groups on the polysaccharide chain of CH can be positively charged and solubilized when the solution pH is below 6, hence becoming a polycationic polymer [13,14]. It has excellent biocompatibility, antimicrobial and wound healing potential as well as hemostatic properties and it has found popular use in the management of burns [15]. Hence, CH is an attractive biomaterial for future use in fabricating functionally graded GTR/GBR membranes [8].

The uses of bioceramic materials alone and as composites with biopolymers have revolutionized the field of regenerative medicine. Synthetic HA has found wide use in tissue engineering applications due to its ability to mimic the natural inorganic bone component showing popular use in composites with other natural and synthetic polymers. The main advantages of HA are its good osteoinductive, osteoconductive properties and excellent biocompatibility [16]. However, its brittleness makes it difficult to shape or bind together. HA composites also impart the formation of a biologically active carbonated HA layer on their surface which is structurally and chemically similar in properties to the mineral phase of bone and enhances interfacial bonding in between tissues and biomaterials [17–19]. Composites of HA have shown to encourage bone cell attachment and proliferation as well as increased mechanical properties compared to the individual components [17,19]. CH can be molded into various patterns of fibers, thin films, and porous structures [20].

Numerous techniques have been used for the fabrication of porous cell-supporting membranes such as particulate leaching, phase inversion and freeze drying. However; drawbacks include difficulty in controlling the pore size, low interconnectivity, and residual salt and skin formation. Another method reported by Ho et al. [20] is freeze gelation (FG). This involves freezing a polymer solution to create frozen solvent and concentrated polymer phases, this phase separation mechanism being referred as solid–liquid demixing [20]. The solvent is extracted by a non solvent and the remaining space becomes porous, resulting in a polymer membrane. Various pore structures and morphologies can be achieved by varying the cooling rate, adjusting the polymer concentration, and changing the solvent system [20,21]. The technique of freeze gelation has also been reported to offer a more convenient, time and energy-efficient method to fabricating porous membranes compared with freeze-drying and offers an easy to scale up process [21]. The freezing process can be carried out in a more controlled

manner to orient the growth of ice crystals in a particular direction [22,23]. More recently Park et al. have used directional freeze-casting with gelatine to mimic topographies with angular similarities of the alveolar crest and natural orientation of periodontal ligaments [24].

In this study, porous FG membranes of CH and CH–HA composites were prepared using two different solvents, ascorbic acid (ASa) and acetic acid (ACa). The preparation and biophysiochemical properties of these porous membranes are herein described with detailed characterization using scanning electron microscopy (SEM), micro computerized tomography (μCT), Fourier transform infrared spectroscopy (FTIR), swelling analysis, degradation studies and tensile testing. Membranes were also examined for their ability to support bone cell growth and matrix deposition by osteogeneic progenitor cells.

2. Materials and methods

2.1. Membrane fabrication

Chitosan (75–85% deacetylated, Sigma Aldrich, UK) having a molecular weight of 190–310 kDa was dissolved in 0.2 M L-ascorbic acid (ASa) (99.9%, Sigma Aldrich, UK) or 0.2 M acetic acid (ACa) (Fisher Scientific, UK) to create 3% w/v solutions with or without HA. This solution was kept stirring for 6 h before adding HA. HA was of medical grade, Captal S™ obtained from Plasma Biotal Limited, UK, (Batch No. P220), incorporated in a ratio of 50:50. After addition of HA, solutions were stirred for 12 h at room temperature and then cast into a petri dish before storing at 4 °C for 3 h and then at −20 °C for 12 h. A solution of Sodium hydroxide 3 M in 100% ethanol in a ratio of 1:1 (v/v) was pre-cooled to −20 °C and used to submerge frozen membranes for 12 h. Membranes were then washed with PBS (Oxoid PBS Tablets, used with distilled water to obtain a 100 mM solution, UK) to elude the remaining neutralizing solution and specimens were dried using a series of ethanol washes (70%, 80%, 90%, 95% and 100%) for 15 min each. After this the samples were immersed in a solution of glycerol (Fisher Scientific. UK) and distilled water in a ratio of 1:10 for 15 min and removed to air dry and stored at room temperature. In total four different membranes were fabricated denoted as ASa-CH, ASa-CH:HA, ACa-CH and ACa-CH:HA. Graphical illustration of a tri-layered GTR membrane is presented in Fig. 1.

2.2. Scanning electron microscopy (SEM)

SEM was employed to study the surface and cross sectional morphology of FG membranes (spot size: 3.0, voltage range 5–10 kV, Philips X-L 20 microscope). Samples were mounted on aluminum stubs with double-sided carbon adhesive dots and were sputter coated under vacuum with carbon using Speedivac carbon coating unit (Model 12E6/1598). Image J (National Institute of Health) software was used for measuring the pore sizes from the cross sectional images. The pore size/cell size and strut thickness were calculated using μCT (Skyscan 1172, Skyscan B.V., Koentich, Belgien). The X-ray tube was equipped with a tungsten target and operated at a voltage of 80 kV and a current of 100 μA. Exposure time per slice was 665 ms. Specimens were rotated through 360°, with one step per degree.

2.3. Fourier transform infrared (FTIR) spectroscopy

FTIR spectra of CH:HA membranes were obtained using a Thermo Nicolet iS50™ FTIR (Thermo Fisher Scientific Inc, USA) spectrophotometer in conjunction with a MTech Photo-Acoustic (PAS) sampling cell to allow analysis of neat samples without
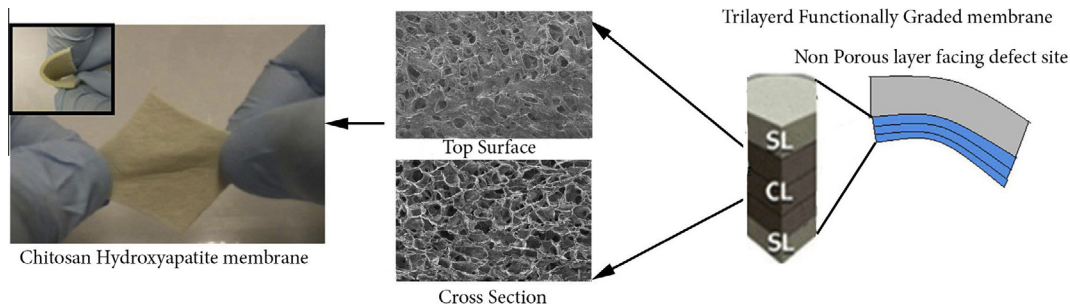
Fig. 1. Schematic illustration of a functionally graded trilayered membrane with the surface layer (SL) and the core layer (CL). Core layer being a FG membrane showing topographical features of the top and cross sectional surface of the membrane and adjacent image showing handling (stretching and bending) characteristics.

extensive sample preparation. Spectra were obtained in the mid-infrared region (4000–400 cm^{-1}) at 4 cm^{-1} resolution accumulating 256 scans. The sample chamber of the PAS cell was purged with dry helium gas. A background scan was obtained before each set of tests using a carbon black specimen. Spectral data were acquired and processed using OMNIC 9™ software.

2.4. Swelling ratio analysis

Samples disks (13 mm Ø) were dried and weighed before storing in PBS at 37 °C to allow any swelling to occur. At set time intervals, samples were removed from PBS and any excess water on the surface was removed with tissue paper before weighing samples. Time intervals used were 0, 15, and 30 min and 1, 24, 48 and 168 h. The swelling ratio was calculated using the formula:

$$\text{Swell ratio } \% \ (Q) = (W_w - W_d)/W_d \times 100$$

where dry weight is given as W_d and wet weight is given as W_w.

2.5. Degradation weight loss analysis

Dry samples were weighed and noted as W_o. These were then immersed in degradation media containing PBS and 5 mg/mL of Egg Hen lysozyme (Sigma Aldrich. UK). Samples were incubated at 37 °C for 4, 7, 14, 21 and 28 days. Media was renewed after every 2–3 days and at each time interval samples were washed 3 times with distilled H$_2$O and then dried out thoroughly before weighing them again as W_t. Weight loss was calculated by using the formula:

$$\text{Weight loss } \% = (W_o - W_t)/W_o \times 100$$

2.6. Mechanical properties

Mechanical testing of dry and wet samples were conducted in tension on a BOSE ELF 3200™ (BOSE ElectroForce System groups, BOSE, Minnesota, USA) using a 22.2 N load cell and ramp test at a rate of 0.1 mm/s to failure. From the obtained stress–strain curves, the point at which the samples snapped was used to calculate the ultimate tensile strength (UTS) and the strain (%), while the initial linear gradient was taken as the Young's modulus (E). Specimens were cut into rectangles with dimensions 5 mm × 20 mm × T, where T is the thickness of the membranes in dry and wet conditions.

2.7. Cell culture

Cell culture on FG membranes was conducted using human osteosarcoma cells (MG63s) and human embryonic stem cell-derived mesenchymal progenitor cells (hES-MPs). MG63's were expanded in Dulbecco's modified Eagle's medium (DMEM) (Biosera, Ringmer, UK) supplemented with 10% Fetal Calf serum (FCS) (Sigma Aldrich UK), 2 mM L-glutamine (Sigma Aldrich Life Sciences, UK), 100 µg/mL of penicillin and streptomycin (Sigma Aldrich, Life Sciences UK). hES-MP's were expanded on gelatin (0.1% w/v in distilled water) coated surfaces and cultured in Alpha Minimum essential medium (α-MEM) (Lonza, Verviers, Belgium), supplemented with 10% FCS, 2 mM L-glutamine and 100 µg/mL penicillin and streptomycin. Cells were grown in a humidified incubator at 37 °C with 5% CO$_2$ with fresh media changes performed every 2–3 days. Cells were grown to 90% confluency and then detached via trypsin–EDTA (Sigma Aldrich, UK). MG63s were used between passages 60–65 while hES-MPs were used between passages 3–7. To analyze the viability of osteoblastic cells on different CH:HA membranes, cells were seeded at a density of 250,000 cells per sample using a marine grade stainless steel seeding ring (internal Ø 10 mm). Prior to cell seeding, the FG membranes were sterilized with ethanol for 1 h, washed twice with PBS for 15 min, and then coated with either culture medium for 1 h prior to seeding MG63's or gelatine for 1 h prior to seeding hES-MPs. Cell free membranes were included as controls.

2.8. Alamar Blue® assay

In order to quantify cell attachment and viability, fluorescent measurements of Alamar Blue were obtained after 1, 4 and 7 days. For each time point, cell seeded samples were carefully washed with PBS and 0.5 ml of Alamar Blue® solution (Sigma Aldrich, UK) (diluted 1:10 with PBS) was added followed by incubation at 37 °C for 4 h. Fluorescence was measured at 570 nm using a fluorescence plate reader (Bio-TEK, NorthStar Scientific Ltd, UK). Based on cell metabolic activity the system incorporates an oxidation–reduction (REDOX) indicator that both fluoresces and changes color in response to chemical reduction of the growth medium resulting from cell growth. Reduction related to growth causes the REDOX indicator to change from oxidized (blue) form to reduced (red) form. After the measurements were taken, samples were washed with PBS, fresh media were added and samples were further cultured in the incubator until the next time point.

2.9. Collagen staining

For identification of collagen deposition by cell on the membranes, picro-sirius red staining was performed. Media were removed after 14, 21 and 28 days, and samples were washed with PBS and then fixed with 3.7% formaldehyde for 30 min. After this samples were washed with PBS and Sirius red solution (direct red dye 1 mg/ml in saturated picric acid, both Sigma, UK) was added to fully submerge samples and left for 18 h under mild rocking (20 rpm). Excess dye was washed with distilled H$_2$O and samples were destained for quantitative analysis using a known

volume of NaOH 0.2 M and Methanol (v/v) (1:1) for 15 min. The extracted solution was read for absorbance at 490 nm in a 96 well plate reader.

2.10. Calcium staining

Total calcium deposition by hES-MPs was quantified at day 14, 21 and 28 after seeding. Samples were fixed (see collagen staining) followed by distilled H_2O washes and then application of 1% Alizarin red solution (pH 4.1) (Sigma, UK) at 1 ml per sample for 20 min on a platform shaker. The unbound dye was removed with distilled water washes. For quantification, the stain was extracted using a known volume of 5% v/v perchloric acid to each well for 30 min. The extracted solution was read for absorbance at 405 nm. Data shown are after subtraction of the absorbance reading obtained on blank scaffolds.

2.11. Histology

Histological samples were prepared from the cross section of unseeded and hES-MP-seeded FG membranes. Samples were fixed with 3.7% formaldehyde and washed 3 × PBS for 15 min each. They were then embedded in paraffin wax and 5 μm sections were obtained with a Leica Microtome, and stained for Hematoxylin and Eosin (H&E). Samples were observed with a Leica optical microscope using Kohler illumination at 20× objective magnification and scaled at 100 μm.

2.12. Statistical analysis

Unless stated otherwise, all experiments were conducted at least three times in triplicate. All presented data refer to mean ± standard deviation (SD). In order to check for any statistically significant differences, a one-way ANOVA was performed followed by Tukey's post hoc test. Results with p-values of $\leqslant 0.05$ (*) were considered statistically significant. All data were analyzed using Graphpad Prism 5.0 software.

3. Results

It is very important to evaluate the physical handling of the membranes and it was passed on to a dental surgeon to analyze its handling properties.

Fig. 2 shows representative images of FG CH and CH:HA membranes being stretched and inset images depict their ability to withstand bending forces. These are both important parameters while handling and inserting during surgical procedures. Thickness of the membranes can be controlled by controlling the amount of similar concentration of the solution poured into the same size of petri dishes. In this study, ACa-CH (3% w/v) solution was prepared and 30 ml was poured into a 9 cm diameter petri dish to obtain a 0.57 mm thick membranes. Membranes could also be easily cut with a scalpel or scissors to obtain the desired shape. These images in Fig. 2 show that all membranes had good handling characteristics and are resilient and flexible.

3.1. Ultra structure of FG membranes by SEM

SEM images of surface and cross-sectional microstructures of CH freeze gelated membranes and pore distribution graphs are shown in Fig. 3. Cross sectional surface of the membranes made with ACa-CH show uneven porous structure as compared to those prepared with ASa-CH. Membranes prepared with HA show the presence of HA crystals over the surface. HA reinforced CH membranes showed fewer pores emerging on the top surface when
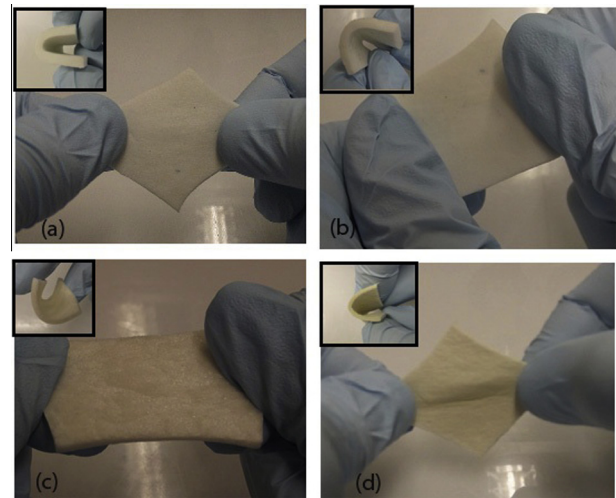

Fig. 2. Optical images taken with Nikon DSLR D5600 camera using macro lens, (a) ACa-CH, (b) ACa-CH:HA, (c) ASa-CH, (d) ASa-CH:HA, all images depicting handling characteristics and the INSET image showing the bending ability of the FG membrane.

compared to neat CH membranes. Data from μCT shown in Fig. 3(I and J) depict the pore size variation from 30 μm to 400 μm and inter strut size ranging from 15 μm to 100 μm. ACa-CH possessed 85% porosity as compared to that of ASa-CH having 79%. Samples containing HA has 78% lower porosity which was relatively lower to ACa-CH and similar to that of ASa-CH. This may be due to the incorporation of HA particles within the network structure of chitosan resulting in closing of pores, hence, lowering the porosity.

3.2. FTIR spectroscopy

FTIR spectroscopy coupled with a photo-acoustic sampling (PAS) cell was utilized to obtain chemical structural properties of neat chitosan and hydroxyapatite individually and to understand the interactions of HA with CH. FTIR-PAS is an excellent technique for obtaining chemical structural properties from the bulk material.

FTIR Spectra of neat CH and HA are shown in Fig. 4 (top), whereas spectra obtained from FG CH membranes and their combinations with HA are shown in Fig. 4 (bottom). Typical spectral bands of N—H and OH stretching vibrations are present within the range of 3600–3300 cm^{-1}. Spectral band at 2880 cm^{-1} is attributed to C—H stretching. Amide I stretching vibration is observed at 1654 cm^{-1} denoted to C=O, Secondary amide II (–NH$_2$) bending vibration is confirmed from 1542 to 1547 cm^{-1}. Moreover, C—H stretching or rock and bending modes were noticed at 1419 cm^{-1} and 1378 cm^{-1}, pyranose v_3 C—O—C (glycosidic linkages) and C—O stretching modes were detected at 1150 cm^{-1} and 1084 cm^{-1}. HA incorporated membranes presented in (Fig. 4c and d) and the presence of HA was confirmed by the hydroxyl peak (–OH) centered at 3568 cm^{-1}, characteristic peaks of v_1 (PO$_4^{3-}$) at 962 cm^{-1}, and v_4 (PO$_4^{3-}$) asymmetric bending stretch at 571 cm^{-1}. Spectral peaks and their interpretation are summarized in Table 1.

3.3. Swelling percentage

The swelling ratio of CH and CH:HA membranes for both solvent systems are shown in Fig. 5a. Equilibrium is reached within 15 min of swelling for most of the freeze gelated CH membranes. ACa-CH and ASa-CH showed the highest swelling ratio (up to
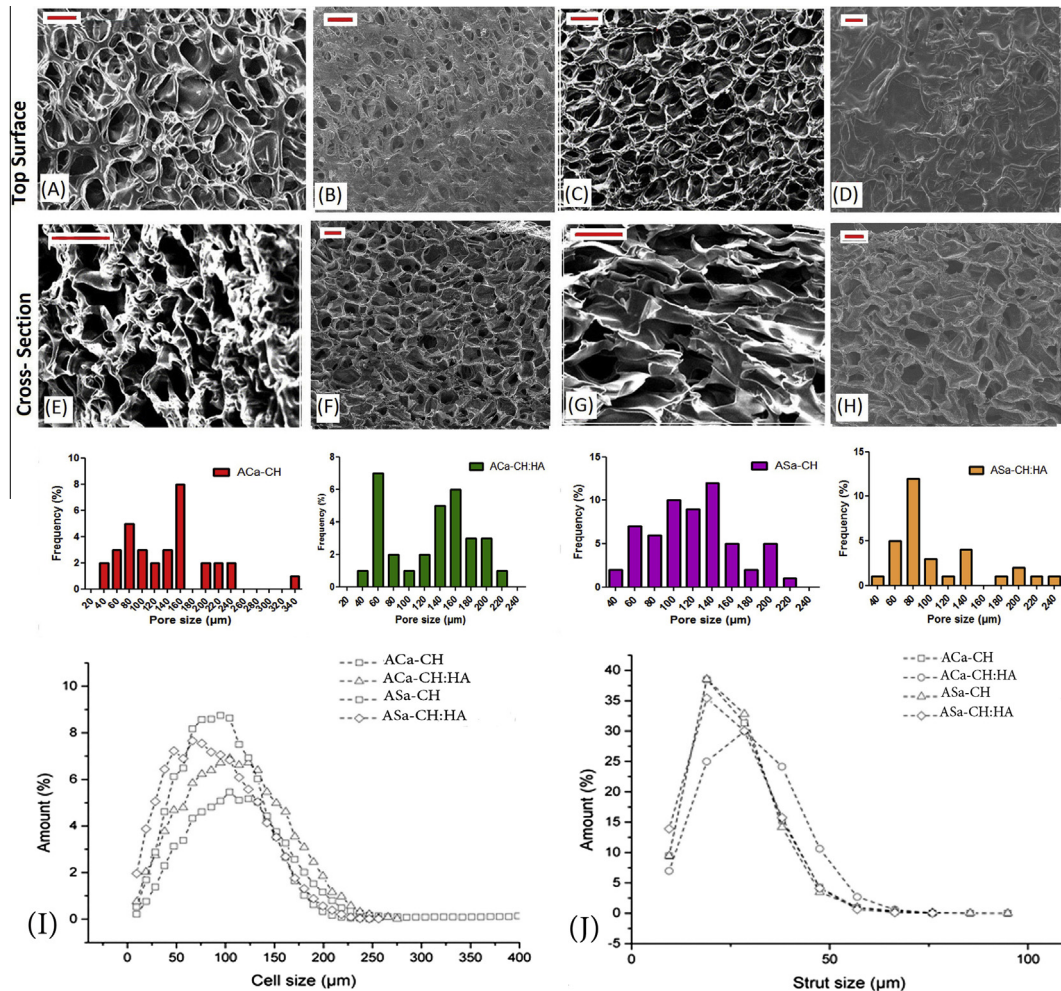
Fig. 3. SEM micrographs of porous FG chitosan (a) top surface of ACa-CH scaffold (b) top surface of ACa-CH:HA (c) top surface of ASa-CH (d) top surface of ASa-CH:HA 50:50HA (e) cross sectional image of ACa-CH (f) cross sectional image of ACa-CH:HA (g) cross sectional image of ASa-CH (h) cross sectional image of ASa-CH 50:50HA. (Scale bar = 100 μm), and (below) a histogram of the pore diameters ($n = 100$). Note that the axis for each histogram is set to different scales depicting the variability in pore diameters in between the scaffold. (I) Graphs depicting percentage porosity plotted against size (μm) and (J) inter strut thickness obtained by μCT analysis, porosity percentage calculated as ACa-CH 85.50%, ACa-CH:HA 77.75%, ASa-CH 78.51%, ASa-CH:HA 78.27%.

80%) when compared with ASa-CH:HA and ACa-CH:HA (up to 60–65%). The swelling profile remained constant over the 48 h time period. ACa-CH:HA membranes showed the least amount of swelling (up to 60%) over the experimental period. Representative images depicting the swelling ability of ACa-CH:HA and ASa-CH membranes are shown in Fig. 5c for both dry and hydrated specimens. Note that membranes incorporating HA showed less swelling as compared to ASa-CH membrane.

3.4. Weight loss analysis

The weight loss (%) profiles of FG membranes immersed in lysozyme solution for a period of 28 days are shown in Fig. 5b. ASa-CH and ACa-CH showed similar degradation profiles across the 28 days showing a weight loss of ~50% at day 4 and ~60% at day 28. The addition of HA to the membranes resulted in a reduction in weight loss for membranes produced from both solvents, however this was more dramatic for ACa-CH:HA which showed the least amount of weight loss at 30–40% between days 7 and 28. In between days 0–4 statistically significant difference ($p \leqslant 0.05$) (α^*) was observed between these two time points. From day 0 and 28 significant difference was noted (β^*). Within groups ACa-CH and ACa-CH:HA showed statistically significant ($p \leqslant 0.05$) difference at day 28. No significant difference was observed in

between ASa-CH:HA and ASa-CH at the 28th day of the experimental period.

3.5. Mechanical properties

Dry and wet FG membranes were analyzed for their ultimate tensile strength (UTS), Young's modulus of elasticity (E) and strain (%) at UTS (Fig. 6). E and UTS values were higher for all dry membranes as compared to specimens in wet conditions. UTS of dry ACa-CH:HA was higher than neat ACa-CH membranes, whereas, E values of dry ACa-CH:HA were lower than neat ACa-CH FG membranes, however, this trend was revised under wet conditions. Dry ASa-CH had a lower E as compared to ASa-CH:HA. Interestingly, under wet conditions ASa-CH:HA membranes had a lower UTS than neat ASa-CH, although there was no significant difference in the E values of these membranes. Examples of stress strain curves of dry and wet FG membranes are shown in Fig. 6a and b.

3.6. Alamar Blue assay

Alamar Blue analysis of FG CH:HA membranes seeded with MG63 or hES-MP cells is represented in Fig. 7(a and b). An increase in cell viability was seen in all the membranes from days 1 to 7
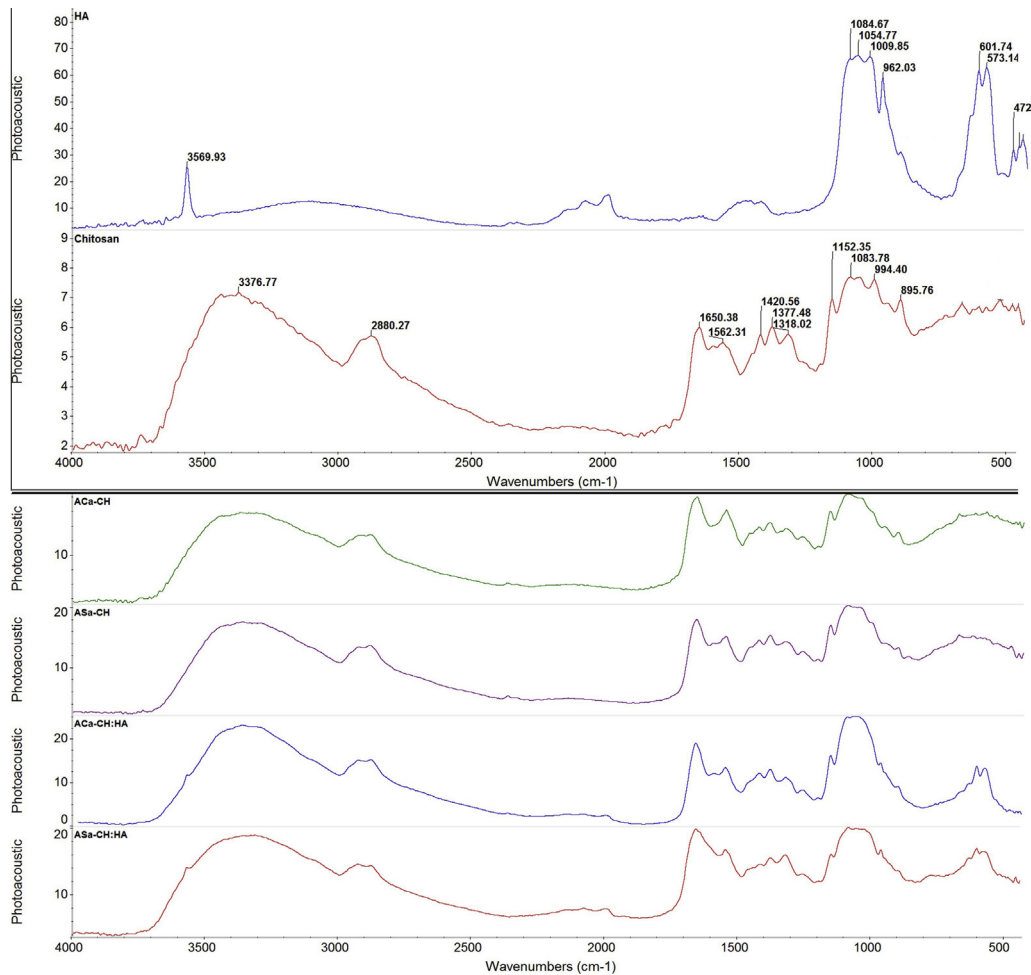
Fig. 4. FTIR spectra of neat medium mol weight chitosan, neat hydroxyapatite with peak identification, FTIR spectra of ACa-CH, ASa-CH, ACa-CH:HA, ASa-CH:HA. Molecular fingerprint region of the HA composite scaffold shows the presence of phosphates bands of HA integrated with CH, small shoulders in HA incorporated spectra is also indicative of intramolecular hydrogen bonding.

(statistically significant) for both cell types, except for ACa-CH (Fig. 7a) cultured with MG63 from days 4 to 7, which showed a non-significant increase. This indicates that the cells were able to attach and proliferate on CH and CH:HA membranes over the course of the culture period. Cell viability was similar at day 1 for all membranes, suggesting that cell attachment was also similar across all membranes. At day 7 of culture, MG63 seeded ACa-CH:HA membranes showed the highest viability (although not statistically significant) when compared with other groups. For membranes cultured with hES-MPs (Fig. 7b), ASa-CH:HA and ACa-CH showed the highest viability at day 7 but this was not statistically significant when compared between groups.

3.7. Collagen and calcium deposition

To analyze the ability of CH-based FG membranes to facilitate osteogenic mineralized-matrix deposition by hES-MPs, quantification of total secreted collagen and calcium was performed at days 14, 21 and 28 of culture. Collagen deposition increased on all membranes from days 14 to 28 (Fig. 7c). Collagen production on ASa-CH:HA was highest at all time points with the highest absorbance value noted on day 28 (statistically significant) compared with all other groups.

Calcium deposition (Fig. 7d) increased in all membranes from days 14 to 28 with the greatest increases seen in both HA composites (significant compared with CH membranes). At day 28 Alizarin

absorbance was highest for ASa-CH:HA although this was not significant when compared with ACa-CH:HA. ACa-CH:HA showed a more gradual increment in calcium deposition from days 14 to 28, whereas, ASa-CH:HA peaked at day 21.

3.8. Histology of chitosan FG membranes

H&E staining of FG control scaffold and CH/CH:HA membranes seeded with hES-MPs are shown in Fig. 8. Cells can be seen within the pores of all membranes. HA-composites appeared to show clumps of cells dispersed throughout the membrane pores, whereas neat CH membranes appeared to show individual cells. ASa-CH:HA membranes (Fig. 8e) contained clumps of cells that were much larger than ACa-CH:HA cell clumps. ASa-CH membranes showed a layer of cells at the surface with fewer cells located beneath the surface in the pores compared with other membranes. ACa-CH:HA membranes also showed cells dispersed within the construct indicating that the cells penetrated through the depth of the membrane. H&E images suggest interconnectivity of the pores within the CH-based constructs due to linking of pores and good cell penetration.

4. Discussion

The regeneration of periodontal tissues lost as a consequence of destructive periodontitis remains a challenge for clinicians, and

Table 1
Fourier transform infrared spectral band assignments.

| Spectral position (cm^{-1})	Assignments	References
Neat chitosan peaks (medium mol. wt.)		
3354	–NH group stretching vibration	Thein-Han et al. [25]
3450	–OH group	Thein-Han et al. [25]
2872–2920	CH$_2$ symmetric and asymmetric stretching vibrations	Manganti et al. [26]
1650	C=O in amide group (amide I)	Cheng et al. [27]
1562	–NH bending vibration in the amide group	Mucha et al. [28]
1590	–NH$_2$ bending in the Amine group	Mucha et al. [28]
1420	CH$_3$ bending deformation (pyranose ring) (C—H)	Thein-Han et al. [25]
1318–1377	CH$_3$ in the amide group, CH bending, CH stretching	Manganti et al. [26]
1252–1255	Free primary amine at C2 position of glucosamine	Thein-Han et al. [25]
1152–1080–1040	Glycosidic linkages (symmetric and asymmetric stretching vibration (C—O—C))	Manganti et al. [26] Cheng et al. [27]
895	Assigned to polysaccharide structure	Siddiqui et al. [30]
599	Bending vibration of amide group	Manganti et al. [26]
Pure hydroxyapatite peaks		
3569	Hydroxyl stretch ν (–OH) on lattice sites of the HA crystal	Rehman and Bonfield [29] Maganti et al. [26] Thein-Han and Misra [25] Rehman et al. [29]
1084–1054	Phosphate (PO$_4^{3-}$) ν$_3$	
962	Phosphate (PO$_4^{3-}$) ν$_1$	
601–573	Phosphate (PO$_4^{3-}$) ν$_4$ Bending deformation	
472	Phosphate (PO$_4^{3-}$) ν$_2$	
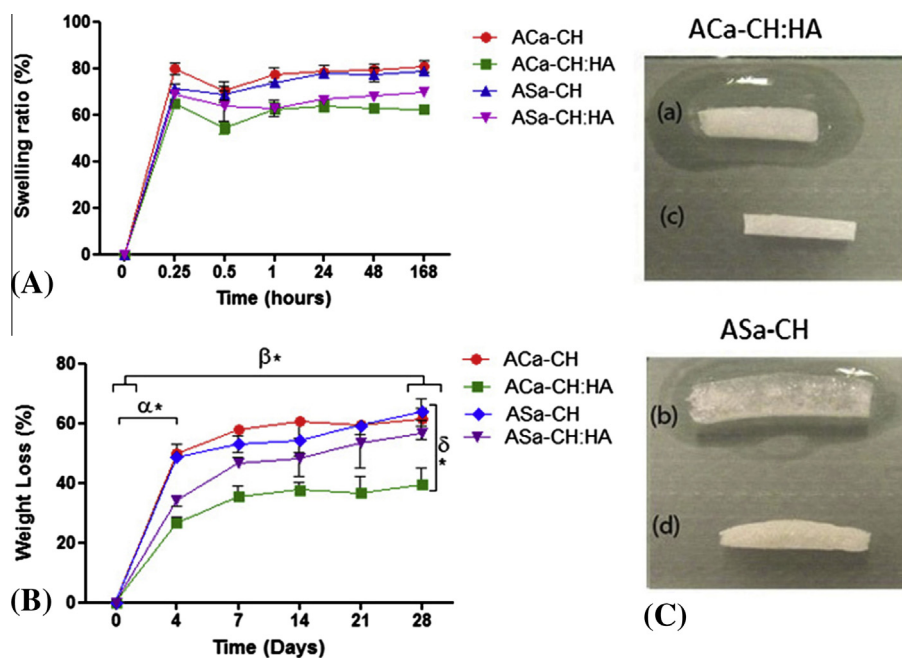
Fig. 5. (A) Swelling ratio of CH FG membranes over 168 h plotted against percentage swelling. Adjacent image (C) show examples of wet (a, b, fully swollen) (top) and dry membranes (c, d) observed from the cross section. (B) Weight loss (%) of FG ACa-CH, ACa-CH:HA, ASa-CH and ASa-CH:HA conducted over a 28 day time scale. Each value represents mean ± SD (n = 3). (α*) Statistically significant difference was noted in between time points from D0 to D4, (β*) statistically significant difference was observed from time point D0 to D28. Within groups at D28 ACa-CH:HA and ACa-CH showed significant difference (δ*).

researchers have explored the possibilities of using biopolymers and bioceramics in regenerating periodontal apparatus. Bearing in mind the proposal by Bottino et al. of having a functionally graded approach to mimic natural structural and functional conditions, we have been able to prepare a membrane that could function as a core structure of a trilayered membrane. The use of the relatively simple technique of freeze gelation has allowed the fabrication of porous composite membranes, which support osteogenic cell viability and matrix deposition. To the best of our knowledge, the formation of porous CH:HA membranes using the reported solvent systems via freeze gelation are yet to be reported and show great potential for use as GTR membranes.

ACa and formic acid have been used as the most common solvents for dissolving CH; other organic acids used include maleic acid, citric acid, tartaric acid, lactic acid and ASa (a vitamer of vitamin C) [13,14,30]. FG membranes of CH prepared by dissolving in ASa showed an increase in tensile properties and water uptake properties compared with ACa-CH membranes, this is an essential property as a periodontal GTR membrane would eventually be surrounded by blood and other body fluids during surgical placement [14]. ASa or Vitamin C in biological systems plays the role of an antioxidant, it not only provides protons to dissolve CH but also acts as a cross linker to improve inherent properties of the ultra structure itself [12,14].

Dry Membranes	Stress (MPa)	E(MPa)	Strain(%)
ACa-CH	0.11±0.05	0.28±0.12	0.46±0.09
ACa-CH:HA	0.13±0.05	0.26±0.09	0.59±0.09
ASa-CH	0.15±0.08	0.20±0.07	0.75±0.19
ASa-CH:HA	0.13±0.03	0.29±0.04	0.50±0.10

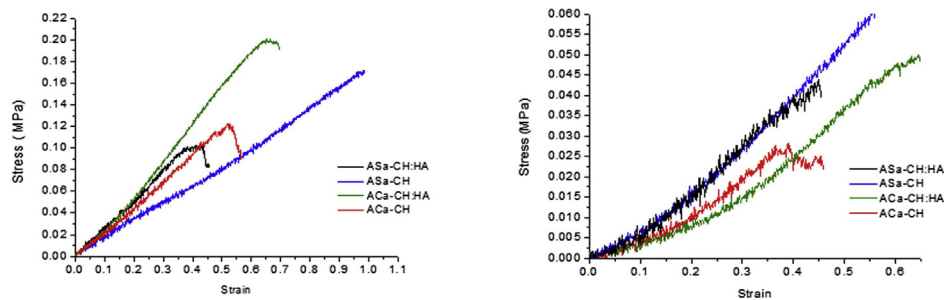| Wet Membranes	Stress (MPa)	E(MPa)	Strain(%)
ACa-CH	0.04±0.03	0.07±0.01	0.38±0.04
ACa-CH:HA	0.06±0.02	0.12±0.03	0.64±0.04
ASa-CH	0.06±0.03	0.10±0.03	0.68±0.04
ASa-CH:HA	0.03±0.01	0.11±0.02	0.35±0.05

Fig. 6. Examples of stress/strain curves obtained from tensile testing (a) dry and (b) wet FG CH membranes. Mechanical properties were calculated for ultimate tensile strength (UTS), Young's modulus (E), strain at UTS (%), data shown are mean ± SD (n = 6).
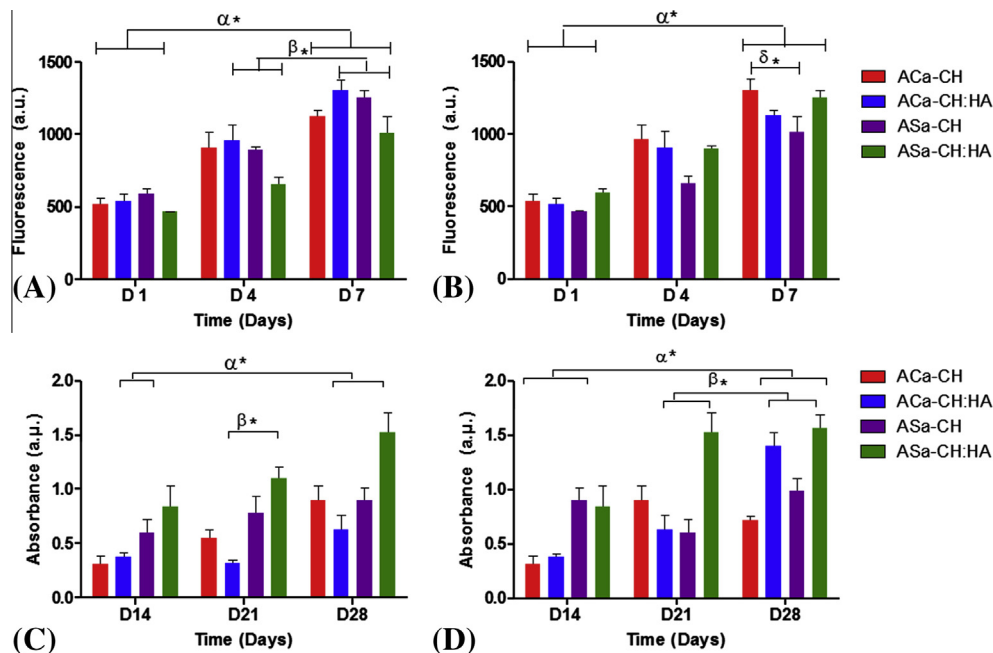

Fig. 7. Metabolic activity using Alamar Blue of CH FG membranes with (a) MG63s and (b) hES-MPs over a period of days 1, 4, and 7. The values are shown as mean ± SD (n = 6). α* denotes significant different between D1 and D7 ($p \leqslant 0.05$). β* denotes significant difference between groups on D4 and D7 (MG63), δ* denotes significant difference between groups at D7 (hESMPs), (c) collagen deposition assessed at day 14, 21 and 28 day of seeding with hESMPs. (d) Calcium deposition on FG CH membranes on Days 14, 21 and 28 of seeding with hES-MP. Values are shown as mean ± SD (n = 6), * denotes statistically significant difference between D14 and D28, between the same groups $p \leqslant 0.05$.

A crucial step in the success of a GTR membrane is the placement of GTR membranes during surgical procedures. The images in Fig. 2 give an indication of the flexibility and resilient nature of these membranes, which should facilitate membrane placement. The membranes showed a porous microarchitecture and some possibility of interconnectivity providing space for vascularization as
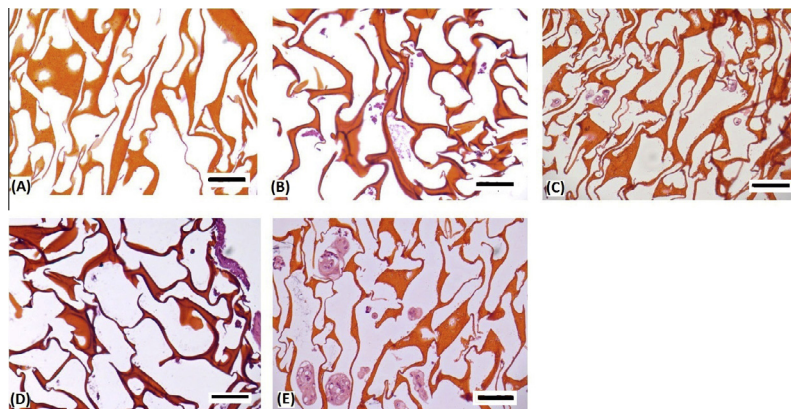
Fig. 8. Cross sectioned H&E staining performed on FG membranes seeded with hES-MPs (a) control specimen, (B) ACa-CH, (C) ACa-CH:HA, (D) ASa-CH, (E) ASa-CH:HA. Images scaled at 100 μm.

seen in Fig. 3. The ultrastructure of the specimens made with ACa-CH was consistent with the work reported previously [14,20]. It was observed that using ASa for dissolving CH resulted in a more even distribution of pores compared with ACa-CH. The relationship between pore size distribution in scaffolds and the effect of this on cellular activity is not-well understood. It has been reported that the minimum recommended pore size for a scaffold is 100 μm to achieve adequate vascularization of the tissue/organ being repaired or regenerated [31]. However, other studies have shown enhanced osteogenesis for implants with pores around 300 μm [32]. Membranes prepared with neat CH dissolved in ACa-CH had the smallest pore diameter and highest porosity percentage as confirmed by μCT data (Fig. 3I and J) and those made with ASa-CH and HA showed larger but even pore sizes. Another study performed by Zoldners et al. has reported the influence of ASa on the stability of CH solutions and has shown that CH accelerated the ASa oxidation process in solution and tends to lower the activation energy of the reaction [33]. It has been reported that pore size and micro architectural geometry of pores in a scaffold can be controlled by managing thermal gradients. A sudden change or a gradual decrease in temperature will affect the geometry and morphology of pores. These slight changes can result in membranes possessing an even porous structure if the freezing temperature is gradually managed or uneven porosity if sudden changes in temperature take place [34]. In our study, it was observed that freeze gelation was effective in producing consistent porous features. However, further in depth knowledge of crystallization of solvents at various freezing rates and fluid dynamics is needed when pouring non-solvent onto frozen CH:HA solution. Decreasing the temperature to −40 °C or −80 °C could possibly give smaller dimensions of pores. Recently Siddiqui et al. have reported that, by addition of micro and nano tricalcium phosphate to CH FG scaffolds, they were able to achieve 77–81% porosity, these measurements were made by mercury intrusion porosimetry [35].

To understand the type of chemical bonding and the functional groups interactions, FTIR in conjunction photoacoustic sampling accessory was employed to study chemical structural properties of bulk membranes. This is advantageous compared to other analyzing techniques such as attenuated total reflectance (ATR) or diffuse reflectance (DRIFT) which are routinely used to study molecular interactions and vibrations only for surface features [29]. By using PAS cell, neat samples without the need of sample preparations can be analyzed.

Spectral data of CH membranes (Fig. 4 bottom image) prepared with ASa-CH and ACa-CH have shown typical Chitosan peaks at (3308, 2880, 1652, 1562, 1420, 1377, 1152 and 1040 cm^{-1}) and

their interpretations are summarized in Table 1. A decrease in intensity of amide I band at 1562 cm^{-1} was observed in the FTIR spectra of CH and HA membranes indicating that there were possible interactions between PO_4^{3-} of HA and NH of CH, which has also been reported by Cheng et al. [27], as changes in the phosphate spectral band at 962 cm^{-1} (assigned to P—O symmetric stretching), 472 cm^{-1} and 601 cm^{-1} denoted to phosphate (v2 and v4 bands of HA respectively) in the spectra of composite membranes point toward possible covalent interactions with CH. FTIR spectrum of HA has a strong OH band at 3568 cm^{-1}), which reduces in intensity when incorporated in CH (Fig. 4). In addition, changes in wavenumber position of polar groups of CH also suggest that hydroxyl ions on the surface of HA might interact with plentiful amino and hydroxyl ions of Chitosan by the formation of hydrogen bonds.

It has also been reported that there might be coordination bonds in between –NH$_2$ of chitosan and Ca^{2+} of HA. Since calcium ions have a coordination number of 7 they are strictly held in structure [27,36]. This coordination bonds have also been reported by Yamaguchi and co-workers as well [37]. In another study on the synthesis of porous chitosan hydroxyapatite composites for tissue engineering by Kim and co-workers, it has been reported that during the composite process chitosan encloses the HA particle inside the polymer [37,38]. Furthermore; they also mentioned that c-axis of the HA crystal tends to align itself along the chitosan chains. Changes in the OH, NH, amide I and phosphate spectral bands confirms possible interactions between the functional groups of HA and CH.

The swelling ratio is also an important parameter for GTR membranes as in clinical use these would be placed in a periodontal defect and covered by the gingival tissue during a surgical flap procedure. The swelling ratio may vary according to the percentage porosity, morphology of pores and membranes ability to uptake and hold water. For periodontal application the degree of swelling is important as the space occupied by the GTR membrane is limited. A further factor to consider is that membranes showing a higher water uptake ratio may possibly allow a greater infiltration of cells. Hydrogel type membranes have two aspects to correlate its ability of cells to migrate through the constructs, one aspect is the physical barrier and another being affinity. A negatively charged particle will struggle through a matrix that bears lots of positively charged binding sites (like CH) due to electrostatic interactions among them. CH membranes dissolved in ASa-CH showed a swelling profile of up to 80%, whereas, those made with ACa-CH and HA combinations reached a maximum swelling percentage of 60–70%. The swelling has been attributed to the unfolding of CH molecules [27]. Wet membrane analysis, which mimics conditions at the

periodontal wound site, undergo hydroplastization due to the aqueous solution, this is why the elongation rate is larger and the tensile strength is lower.

Swelling kinetics studied by Silva et al. showed that a higher degree of crosslinking was effective in lowering the equilibrium hydration degree [39]. They used glutaraldehyde as a crosslinking agent and stated that lower crystallinity increases the water molecules accessibility. Ren et al. also studied enzymatic degradation and swelling characteristics of CH matrices and obtained similar findings [40]. A study conducted by Li et al. showed a significant reduction in water uptake of CH and bioactive glass ceramic composite membranes, which is similar to our findings for membranes prepared with ASa-CH that showed a swelling rate of 90% and an addition of HA resulted in decreased swelling [41].

Membrane degradation is important to avoid the need for a second surgical procedure for removal of the membrane, and to allow space for newly formed tissue. Degradation of CH occurs by hydrolysis mainly by lysozymes present in the body and β-1-4N-acetyl glucosamine units of CH undergo chain scission. This phenomenon leads to the release of aminosugars, which can be incorporated into the metabolic pathway or excreted through the body. Peter et al. and Mota et al. reported that the addition of Bioglass™ reduces the degradation rate and they attributed this decrease in weight loss to the neutralization of the acidic products of CH by the alkali groups [31,42]. Our study showed similar findings (Fig. 5b) and it was observed that membranes with no HA showed 50% initial weight loss, whereas, with HA additions it was reduced to 35% after 21 days. Hydrolysis is the basic mechanism of degradation for CH, as interactions with the water molecule breaks the polymer network into smaller chains. Degradation products of the CH include saccharides and glucosamines as part of the normal metabolism process [43] and the breakdown of HA occurs through the resorption process [44]. HA interactions with CH reinforce the composite structure, which results in reduced porosity and are less prone to water uptake giving rise to decreased rate of hydrolysis. This is also evident from the results of swelling ratio, porosity decreases from 85% to 78% with the incorporation of HA. It is envisaged that by tailoring the amount and type of HA to our membrane will allow to control both the swelling ratio and as well as the degradation rate.

Tensile testing under dry conditions is indicative of the handling ability such as bending, flexibility and ease of cutting of membranes by periodontists during manipulation into the defect site while performing a surgical procedure. Analysis in wet conditions resembles the clinical scenario once the GTR membrane is placed in a hydrated environment. Addition of HA to CH membranes made with ASa showed an increase in UTS and E, which may be due to the covalent bonding that formed between the –OH and PO_4 of HA to NH_3^+ of CH. Mota et al. reported the addition of bioactive glass ceramic to CH membranes causes an increase in stiffness under both dry and wet conditions. The strength of the membrane and elongation at failure also tend to decrease with the presence of bioglass nanoparticles [42]. In this study, maximum elongation at failure was seen for CH dissolved in ACa and ASa with HA (Fig. 6). Frohberg et al. [45] have also reported that addition of HA reduces the mechanical strength. This decrease might not occur if HA is dispersed within the polymer chains on or near the surface of the scaffold, this is similar to what we were able to elucidate from our FTIR-PAS data that HA was dispersed throughout the membrane, as HA spectral peaks were observed from different points of the samples analyzed. In addition, the chemical bonding that occurs within the HA particulates and the CH is crucial in improving the mechanical strength of the composite, which was observed in our study, as HA reinforced CH FG membranes demonstrated higher E values as compared to neat CH membranes. It is important to note

that chemical interactions between the CH and HA were confirmed by FTIR spectral data.

Alamar Blue results (Fig. 7a and b) showed an increase in viability for both mature and progenitor osteogenic cells on all the membranes over 7 days of culture. The osteogenic potential of CH and CH:HA membranes have been assessed in a previous study by Frohbergh et al. in which they noticed a decrease in cell metabolic activity over time in HA membranes and attributed this decline to the increased alkaline phosphatase activity [45]. Other studies have observed increasing viability of mesenchymal stem cells (MSCs) on CH:HA composite membranes compared with neat CH membranes [35,46]. The final phase for osteogenic differentiation is matrix mineralization and our analysis after 28 days of hES-MP culture showed that calcium deposition was supported by all membranes but highest on membranes prepared with HA incorporated compared to CH alone. It has been reported in the literature that hES-MP cells deposit HA-like mineral in vitro after 3 weeks of osteogenic differentiation, which was analyzed by using TOF-SIMS and depth profiling [47]. Similar results were observed in this study, where increment of both the calcium and collagen deposition was observed for membranes containing HA (Fig. 7c and d), this could be due to the scaffold providing a more suitable balance of collagen with mineral content. Collagen production was significantly higher on ASa-CH:HA membranes compared with ACa-CH:HA while calcium deposition at day 28 was similar, this could be attributed to leaching of leftover ASa, creating a more suitable environment for collagen deposition. Overall membranes with HA promoted higher mineralized-matrix deposition, and this observation has been seen previously by osteogenic cells in another three dimensional CH:HA membrane culture [48].

hES-MPs are highly representative of bone-marrow derived MSCs in terms of surface marker profile, gene expression and mesodermal differentiation ability and they express no embryonic stem cell markers. They have also been shown to deposit HA-like mineral [47]. They show a higher degree of homogeneity than human bone marrow derived mesenchymal stem cells (h-BMSCs) giving more consistent outcomes. MG63 cells have been widely used to initially test the biocompatibility of new materials for supporting osteogenic growth [49], and it is possible that mature bone cells may be present in the remaining alveolar bone [50]. Periodontal ligament cells were not included in this study as the aims were to fully characterize the membranes physiochemical properties and then investigate their potential to support new bone formation, which is an important first step to then allow ligament anchorage and growth.

Histological analysis performed 7 days (Fig. 8) after seeding the membranes with hES-MPs showed that cells penetrated deep into most membranes. hES-MPs are a more relevant cell type than MG63s in the context of the overall GTR goal, and they represent the MSC that would infiltrate the membrane in vivo [51], therefore histology was only performed on hES-MPs. ASa-CH membranes showed that the majority of cells formed a multilayer on the surface with few penetrating deep into the pores. This could be due to lower degree of interconnectivity or a scaffold-cell interactions hindering their migration into the membrane. ASa-CH:HA membranes showed that cells penetrated through the depth of the scaffold which may be attributed to the presence of HA or the cellular affinity for these particular membranes was improved with ASa-CH and HA combination.

It would be interesting to see how nano HA effects the pore size, distribution and morphology on the overall microstructure of the scaffold. As it is a well established fact that nano-HA possess a higher surface area to volume ratio bearing the capability to achieve tighter interface with polymer composites. Moreover, a higher surface area will cause faster release of ions hence enhancing bioactivity simultaneously encouraging protein adsorption as

well. Nano-HA also resembles the biological apatite due to its ultrafine structure, hence playing a pivotal role in hard tissue replacement [52]. Furthermore, directional freezing process can be employed to assist PDL growth, by controlling the freezing orientation to fabricate sub longitudinal pores with angular similarities to native PDL [24].

5. Conclusion

In this study, porous CH-based membranes with and without HA were prepared using ACa or ASa as solvent systems via the novel and efficient technique of freeze gelation. The CH:HA composites have shown potential for use as a core layer in a functionally graded GTR membrane for periodontal tissue engineering, fulfilling a number of key requirements of satisfactory handling properties for clinicians. Choice of solvent used to dissolve CH and amount of incorporated HA helps in tailor making the physical and chemical properties of membranes. Membranes were resilient to handling during dry and wet conditions that may simulate clinical use. A favorable cellular response was also seen for CH:HA composite membranes suggesting that HA incorporation effects cellular activity. Therefore; this study shows that these porous membranes have a potential to be used as a core layer of a functionally graded structure in periodontal regeneration membranes. Furthermore, freeze gelation technique may be employed in future to create tissue engineering scaffolds for other biomedical applications.

Acknowledgement

Appendix A. Figures with essential color discrimination

Certain figures in this article, particularly Figs. 1–8, are difficult to interpret in black and white. The full color images can be found in the on-line version, at doi: http://dx.doi.org/10.1016/j.actbio.2015.05.001.

References

[1] H. Shimauchi, E. Nemoto, H. Ishihata, M. Shimomura, Possible functional scaffolds for periodontal regeneration, Jpn. Dent. Sci. Rev. 49 (2013) 118–130.
[2] M.C. Bottino, V. Thomas, G. Schmidt, Y.K. Vohra, T.M. Chu, M.J. Kowolik, et al., Recent advances in the development of GTR/GBR membranes for periodontal regeneration–a materials perspective, Dent. Mater. 28 (2012) 703–721.
[3] F.J. Hughes, M. Ghuman, A. Talal, Periodontal regeneration: a challenge for the tissue engineer?, Proc Inst. Mech. Eng. H 224 (2010) 1345–1358.
[4] J. Gottlow, Guided tissue regeneration using bioresorbable and non-resorbable devices: initial healing and long-term results, J. Periodontol. 64 (1993) 1157–1165.
[5] E. Milella, P.A. Ramires, E. Brescia, G. La Sala, L. Di Paola, V. Bruno, Physicochemical, mechanical, and biological properties of commercial membranes for GTR, J. Biomed. Mater. Res. 58 (2001) 427–435.
[6] M.C. Bottino, V. Thomas, G.M. Janowski, A novel spatially designed and functionally graded electrospun membrane for periodontal regeneration, Acta Biomater. 7 (2011) 216–224.
[7] P. Bunyaratavej, H.L. Wang, Collagen membranes: a review, J. Periodontol. 72 (2001) 215–229.
[8] M. Dash, F. Chiellini, R.M. Ottenbrite, E. Chiellini, Chitosan—a versatile semi-synthetic polymer in biomedical applications, Prog. Polym. Sci. 36 (2011) 981–1014.
[9] M. Schwartzmann, Use of collagen membranes for guided bone regeneration: a review, Implant Dent. 9 (2000) 63–66.
[10] R. Muzzarelli, G. Biagini, A. Pugnaloni, O. Filippini, V. Baldassarre, C. Castaldini, et al., Reconstruction of parodontal tissue with chitosan, Biomaterials 10 (1989) 598–603.
[11] R.A.A. Muzzarelli, Chitosan composites with inorganics, morphogenetic proteins and stem cells, for bone regeneration, Carbohydr. Polym. 83 (2011) 1433–1445.
[12] R.A.A. Muzzarelli, F. Tanfani, M. Emanuelli, Chelating derivatives of chitosan obtained by reaction with ascorbic acid, Carbohydr. Polym. 4 (1984) 137–151.
[13] C.K.S. Pillai, W. Paul, C.P. Sharma, Chitin and chitosan polymers: chemistry, solubility and fiber formation, Prog. Polym. Sci. 34 (2009) 641–678.
[14] Po-Hui Chen, Ya-Hsi Hwang, Ting.-Yun. Kuo, Fang-Hsuan Liu, Juin-Yih Lai, Hsyue-Jen Hsieh, Improvement in properties of chitosan membranes using natural organic acid solutions as solvents for chitosan dissolution, J. Med. Biol. Eng. 27 (2007) 23–28.
[15] A.K. Azad, N. Sermsintham, S. Chandrkrachang, W.F. Stevens, Chitosan membrane as a wound-healing dressing: characterization and clinical application, J. Biomed. Mater. Res. B Appl. Biomater. 69B (2004) 216–222.
[16] H. Zhou, J. Lee, Nanoscale hydroxyapatite particles for bone tissue engineering, Acta Biomater. 7 (2011) 2769–2781.
[17] L.J. Kong, Y. Gao, G.Y. Lu, Y.D. Gong, N.M. Zhao, X.F. Zhang, A study on the bioactivity of chitosan/nano-hydroxyapatite composite scaffolds for bone tissue engineering, Eur. Polym. J. 42 (2006) 3171–3179.
[18] A.S. Khan, K.R. Hassan, S.F. Bukhari, F.S. Wong, I.U. Rehman, Structural and in vitro adhesion analysis of a novel covalently coupled bioactive composite, J. Biomed. Mater. Res. B Appl. Biomater. 100 (2012) 239–248.
[19] A.S. Khan, Z. Ahmed, M.J. Edirisinghe, F.S.L. Wong, I.U. Rehman, Preparation and characterization of a novel bioactive restorative composite based on covalently coupled polyurethane–nanohydroxyapatite fibres, Acta Biomater. 4 (2008) 1275–1287.
[20] M.-H. Ho, P.-Y. Kuo, H.-J. Hsieh, T.-Y. Hsien, L.-T. Hou, J.-Y. Lai, et al., Preparation of porous scaffolds by using freeze-extraction and freeze-gelation methods, Biomaterials 25 (2004) 129–138.
[21] C.-Y. Hsieh, S.-P. Tsai, M.-H. Ho, D.-M. Wang, C.-E. Liu, C.-H. Hsieh, et al., Analysis of freeze-gelation and cross-linking processes for preparing porous chitosan scaffolds, Carbohydr. Polym. 67 (2007) 124–132.
[22] S. Deville, R.K. Nalla, Freezing as a path to build complex composites (vol. 312, p. 515, 2006), Science 312 (2006) 1312.
[23] S. Deville, E. Saiz, R.K. Nalla, A.P. Tomsia, Freezing as a path to build complex composites, Science 311 (2006) 515–518.
[24] C.H. Park, K.H. Kim, H.F. Rios, Y.M. Lee, W.V. Giannobile, Y.J. Seol, Spatiotemporally controlled microchannels of periodontal mimic scaffolds, J. Dent. Res. 93 (2014) 1304–1312.
[25] W.W. Thein-Han, R.D. Misra, Biomimetic chitosan–nanohydroxyapatite composite scaffolds for bone tissue engineering, Acta Biomater. 5 (2009) 1182–1197.
[26] N. Maganti, P.K.C. Venkat Surya, W.W. Thein-Han, T.C. Pesacreta, R.D.K. Misra, Structure–process–property relationship of biomimetic chitosan-based nanocomposite scaffolds for tissue engineering: biological, physico-chemical, and mechanical functions, Adv Eng Mater 13 (2011) B108–B122.
[27] X.M. Cheng, Y.B. Li, Y. Zuo, L. Zhang, J.D. Li, H.A. Wang, Properties and in vitro biological evaluation of nano-hydroxyapatite/chitosan membranes for bone guided regeneration, Mater. Sci. Eng. C Biomim. Supramol. Syst. 29 (2009) 29–35.
[28] M. Mucha, A. Pawlak, Complex study on chitosan degradability, Polymer 47 (2002). 519–6.
[29] I. Rehman, W. Bonfield, Characterization of hydroxyapatite and carbonated apatite by photo acoustic FTIR spectroscopy, J. Mater. Sci. Mater. Med. 8 (1997) 1–4.
[30] R. Ravindra, K.R. Krovvidi, A.A. Khan, Solubility parameter of chitin and chitosan, Carbohydr. Polym. 36 (1998) 121–127.
[31] M. Peter, N.S. Binulal, S.V. Nair, N. Selvamurugan, H. Tamura, R. Jayakumar, Novel biodegradable chitosan–gelatin/nano-bioactive glass ceramic composite scaffolds for alveolar bone tissue engineering, Chem. Eng. J. 158 (2010) 353–361.
[32] C.M. Murphy, F.J. O'Brien, Understanding the effect of mean pore size on cell activity in collagen–glycosaminoglycan scaffolds, Cell Adhes. Mig. 4 (2010) 377–381.
[33] J. Zoldners, T. Kiseleva, I. Kaiminsh, Influence of ascorbic acid on the stability of chitosan solutions, Carbohydr. Polym. 60 (2005) 215–218.
[34] A. Macchetta, I.G. Turner, C.R. Bowen, Fabrication of HA/TCP scaffolds with a graded and porous structure using a camphene-based freeze-casting method, Acta Biomater. 5 (2009) 1319–1327.
[35] N. Siddiqui, K. Pramanik, Effects of micro and nano β-TCP fillers in freeze-gelled chitosan scaffolds for bone tissue engineering, J. Appl. Polym. Sci. 131 (2014) 41025–41035.
[36] M. Kikuchi, T. Ikoma, S. Itoh, H.N. Matsumoto, Y. Koyama, K. Takakuda, et al., Biomimetic synthesis of bone-like nanocomposites using the self-organization mechanism of hydroxyapatite and collagen, Compos. Sci. Technol. 64 (2004) 819–825.
[37] I. Yamaguchi, S. Itoh, M. Suzuki, A. Osaka, J. Tanaka, The chitosan prepared from crab tendons: II. The chitosan/apatite composites and their application to nerve regeneration, Biomaterials 24 (2003) 3285–3292.
[38] H.S. Kim, J.T. Kim, Y.J. Jung, S.C. Ryu, H.J. Son, Y.G. Kim, Preparation of a porous chitosan/fibroin–hydroxyapatite composite matrix for tissue engineering, Macromol. Res. 15 (2007) 65–73.
[39] R.M. Silva, G.A. Silva, O.P. Coutinho, J.F. Mano, R.L. Reis, Preparation and characterisation in simulated body conditions of glutaraldehyde crosslinked chitosan membranes, J. Mater. Sci. Mater. Med. 15 (2004) 1105–1112.
[40] D. Ren, H. Yi, W. Wang, X. Ma, The enzymatic degradation and swelling properties of chitosan matrices with different degrees of N-acetylation, Carbohydr. Res. 340 (2005) 2403–2410.
[41] X.Y. Li, K.H. Nan, S. Shi, H. Chen, Preparation and characterization of nano-hydroxyapatite/chitosan cross-linking composite membrane intended for tissue engineering, Int. J. Biol. Macromol. 50 (2012) 43–49.

[42] J. Mota, N. Yu, S.G. Caridade, G.M. Luz, M.E. Gomes, R.L. Reis, et al., Chitosan/bioactive glass nanoparticle composite membranes for periodontal regeneration, Acta Biomater. 8 (2012) 4173–4180.

[43] M.N.V.R. Kumar, R.A.A. Muzzarelli, C. Muzzarelli, H. Sashiwa, A.J. Domb, Chitosan chemistry and pharmaceutical perspectives, Chem. Rev. 104 (2004) 6017–6084.

[44] Y. Shikinami, Y. Matsusue, T. Nakamura, The complete process of bioresorption and bone replacement using devices made of forged composites of raw hydroxyapatite particles/poly L-lactide (F-u-HA/PLLA), Biomaterials 26 (2005) 5542–5551.

[45] M.E. Frohbergh, A. Katsman, G.P. Botta, P. Lazarovici, C.L. Schauer, U.G. Wegst, et al., Electrospun hydroxyapatite-containing chitosan nanofibers crosslinked with genipin for bone tissue engineering, Biomaterials 33 (2012) 9167–9178.

[46] Z.Q. Li, X.J. Tian, Y. Yuan, Z.X. Song, L.L. Zhang, X. Wang, et al., Effect of cell culture using chitosan membranes on stemness marker genes in mesenchymal stem cells, Mol. Med. Rep. 7 (2013) 1945–1949.

[47] G.M. de Peppo, P. Sjovall, M. Lenneras, R. Strehl, J. Hyllner, P. Thomsen, et al., Osteogenic potential of human mesenchymal stem cells and human embryonic stem cell-derived mesodermal progenitors: a tissue engineering perspective, Tissue Eng. A 16 (2010) 3413–3426.

[48] G. Wang, L. Zheng, H. Zhao, J. Miao, C. Sun, N. Ren, et al., In vitro assessment of the differentiation potential of bone marrow-derived mesenchymal stem cells on genipin-chitosan conjugation scaffold with surface hydroxyapatite nanostructure for bone tissue engineering, Tissue Eng. A 17 (2011) 1341–1349.

[49] L. Grausova, A. Kromka, Z. Burdikova, A. Eckhardt, B. Rezek, J. Vacik, et al., Enhanced growth and osteogenic differentiation of human osteoblast-like cells on boron-doped nanocrystalline diamond thin films, PLoS One 6 (2011) e20943.

[50] H. Egusa, W. Sonoyama, M. Nishimura, I. Atsuta, K. Akiyama, Stem cells in dentistry–Part II: clinical applications, J. Prosthodont. Res. 56 (2012) 229–248.

[51] P.N. Mendes, S.C. Rahal, O.C.M. Pereira-Junior, V.E. Fabris, S.L.R. Lenharo, J.F. de Lima-Neto, et al., In vivo and in vitro evaluation of an Acetobacter xylinum synthesized microbial cellulose membrane intended for guided tissue repair, Acta Vet. Scand. 51 (2009).

[52] S. Sowmya, J.D. Bumgardener, K.P. Chennazhi, S.V. Nair, R. Jayakumar, Role of nanostructured biopolymers and bioceramics in enamel, dentin and periodontal tissue regeneration, Prog. Polym. Sci. 38 (2013) 1748–1772.